Macular Imaging

Ki Ho Park and Yong Woo Kim

Abstract

Innovative advances in optical coherence tomography (OCT) imaging facilitate precise exploration and monitoring of macular structures in glaucoma patients. Measurement of ganglion cell layer (GCL) and inner plexiform layer (IPL) thicknesses in the macula provides excellent diagnostic ability for glaucoma comparable to that of peripapillary retinal nerve fiber layer (RNFL) measurement. The thickness and deviation maps provided by OCT devices broadened our understanding of the patterns and temporal relationships of glaucomatous damage in the macular and peripapillary areas. This technology has enhanced the topographical analysis of structural damage to the macula and corresponding changes in the peripapillary region. The macular parameters can facilitate early detection of glaucomatous damage and discriminate meaningful progression in advanced as well as early stages of glaucoma. This chapter provides information from the basics to the latest updates on macular imaging in the field of glaucoma along with relevant clinical cases.

K. H. Park (✉) · Y. W. Kim
Department of Ophthalmology, Seoul National University Hospital, Seoul National University College of Medicine, Jongno-gu, Seoul, Korea
e-mail: kihopark@snu.ac.kr

Keywords

Macular imaging · Ganglion cell layer · Inner plexiform layer · Temporal raphe sign · Macular vulnerability zone · Preperimetric glaucoma

1 Anatomy and Histology for Macular Imaging by OCT

The retina is a multi-layered structure made up of two synaptic (plexiform) layers sandwiched between three nuclear layers: the outer nuclear layer (ONL), inner nuclear layer (INL), and ganglion cell layer (GCL). The ONL contains the cell bodies of photoreceptors (rods and cones), and the INL contains the cell bodies of bipolar, horizontal, amacrine, and radial glial (Müller) cells. The GCL contains displaced amacrine and retinal ganglion cells (RGC). These three nuclear layers are separated by two synaptic (plexiform) layers. The outer plexiform layer (OPL) is located between the ONL and the INL, and is the place where the photoreceptors, horizontal and bipolar cell dendrites interact. The inner plexiform layer (IPL) lies between the INL and GCL and is where the bipolar cell axons, amacrine, and ganglion cells interact. The retinal nerve fiber layer (RNFL) consists primarily of RGC axons.

K. H. Park, T.-W. Kim (eds.), *OCT Imaging in Glaucoma*,
https://doi.org/10.1007/978-981-16-1178-0_3

Optical coherence tomography (OCT) technology has attained improved axial resolution to 5–8 μm. This makes it possible to correlate OCT images in-vivo with histological features of the retina. Despite the fact that the OCT features of the outer retina are less well understood and remain controversial, the features of the inner retina appear to be well correlated with histology. Within the retina, the RNFL and the plexiform layers (both inner and outer) are seen as hyperreflective, while the GCL and the nuclear layers (both inner and outer) are hyporeflective. The retinal blood vessels can be seen in OCT images as circular hyperreflective structures in the inner retina, with a reduced reflectivity that extends into the deeper layers (vertical shadow). A representative OCT image of a human retina with annotated layers is provided in Fig. 1.

The macula is an oval-shaped pigmented area (*macula lutea*) in the center of the retina, about 5.5 mm in diameter in humans. It covers the region surrounding the fovea with the highest density of RGCs (over 30% of RGCs) despite occupying less than 2% of the retinal area. The macular structure is characterized by less variation among individuals, and therefore, is relatively less affected by ocular or demographic factors than is the peripapillary RNFL. Glaucoma is characterized by progressive loss of RGCs, with typical changes in the optic nerve head, resulting in progressive visual field defect in the corresponding area. It has long been well documented that early-glaucomatous damage can affect the macula (Anctil and Anderson 1984; Heijl and Lundqvist 1984). However, clinicians paid less attention to the macula until accurate measurements of each of the retinal layers of the macula became possible in-vivo. Lately, several commercially available OCT devices have made available various types of macular parameters. The two representative macular parameters are the combinations of measurements of the RNFL, GCL, and IPL: the ganglion cell-inner plexiform layer (GCIPL) thickness is the sum of the thicknesses of the GCL and IPL; the ganglion cell complex (GCC) thickness is the sum of the thicknesses of the RNFL, GCL, and IPL. These two parameters are the most commonly used and obviously essential for early detection and monitoring of glaucoma.

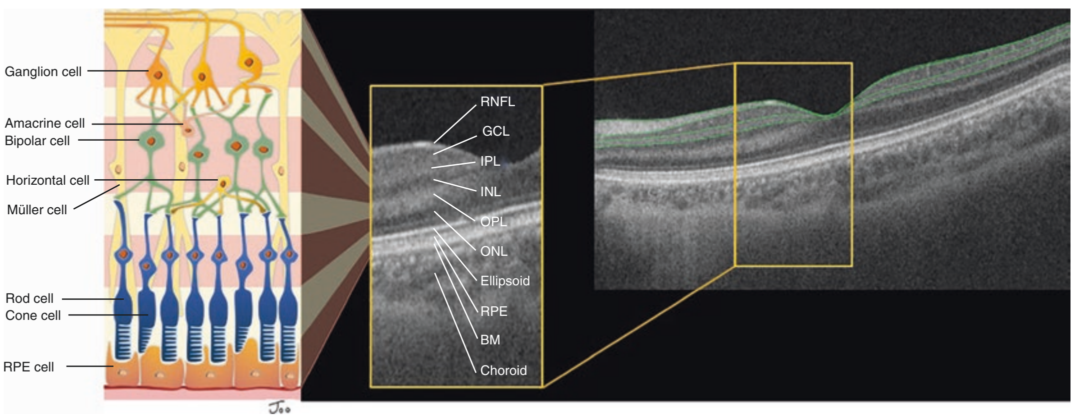

Fig. 1 Human macular structure. Retinal layers (Left) and representative human macular structure imaged by swept-source optical coherence tomography (SS-OCT) (Middle and Right). Retinal nerve fiber layer (RNFL), ganglion cell layer (GCL), and inner plexiform layer (IPL) are annotated in green solid lines. The foveal structure in the yellow inset is magnified and each retinal layer is annotated. RNFL, retinal nerve fiber layer; GCL, ganglion cell layer; IPL, inner plexiform layer; INL, inner nuclear layer; OPL, outer plexiform layer; ONL, outer nuclear layer; RPE, retinal pigment epithelium; BM, Bruch's membrane

2 Topographic Correlations among Optic Nerve Head, RNFL, and Macula

The axons of the RGC lie in the RNFL in bundles and enter the optic disc. The RNFL bundles each have their own course of travel to the optic disc. The RNFL at the temporal side of the fovea travels to the optic disc in an arcuate shape around the fovea. The axons of the RGC do not cross the horizontal meridian, so that a raphe with relatively few axons is formed in the temporal area (temporal raphe). According to this anatomy, most macular change in glaucomatous eyes appears in an arcuate-to-crescent shape, and is located mainly in the temporal macular regions along the horizontal raphe. The macular change also is usually located within the same hemifield on the continuum of the corresponding RNFL defect and optic disc damage (Fig. 2).

It is widely accepted that glaucomatous defect is most prevalent in the inferotemporal and superotemporal regions of the optic disc. The neural canal opening is connected to the superonasal region of the eyeball. This means that the center of the optic disc lies about 6° above the horizontal midline through the center of the fovea.

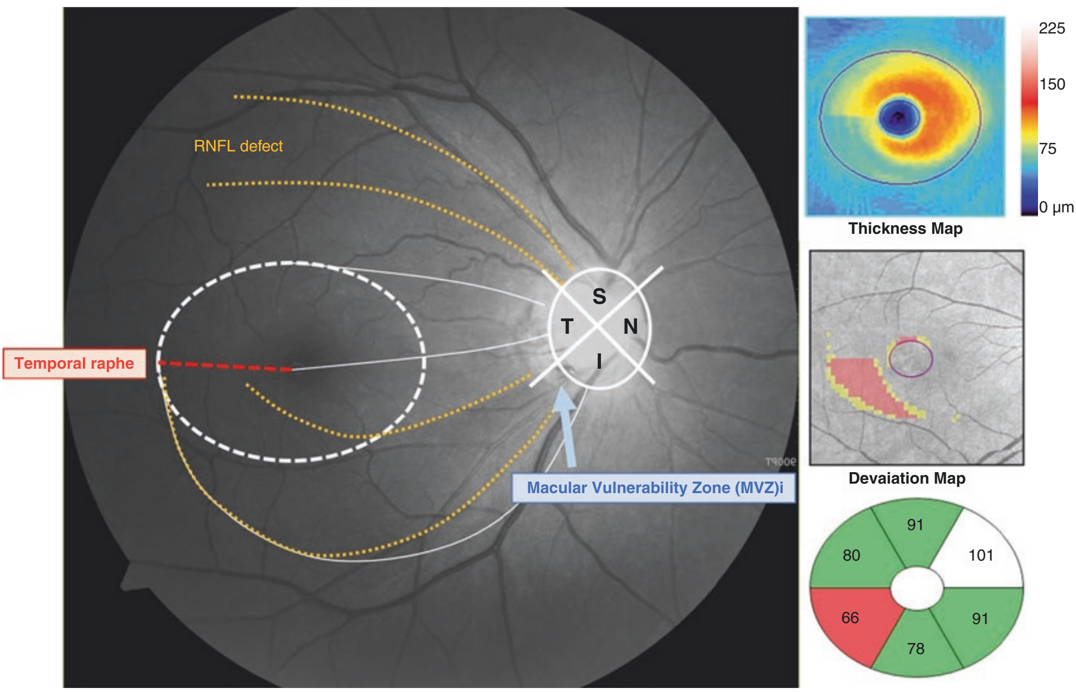

Fig. 2 Macular damage in glaucoma. The axons of the retinal ganglion cells (RGC) travel in the retinal nerve fiber layer (RNFL) in bundles and enter the optic disc. The RNFL at the temporal side of the fovea travels to the optic disc in an arcuate shape around the fovea. The RGC axons do not cross the horizontal meridian, so that a raphe with relatively few axons is formed in the temporal area (temporal raphe, red dotted line). RGC axons in the superior macula enter through the temporal border of the optic disc while RGC axons in the inferior macula enter through the inferotemporal border of the optic disc. This topographical relationship between the macula and the optic disc results in an overlap of the inferior macular region with the inferotemporal region of the optic disc, where glaucomatous defects dominate. Hood et al. designated this region the "macular vulnerability zone (MVZ)" of the optic disc (blue arrow). Case of 40-year-old male with primary open-angle glaucoma (POAG) in right eye. Note the inferotemporal and superotemporal RNFL defects in the red-free RNFL photography. Thickness and deviation maps for the ganglion cell-inner plexiform layer (GCIPL) from Cirrus HD-OCT (Carl Zeiss Meditec, Dublin, CA, USA) are provided. Macular damage is manifest in the inferotemporal macular region (inferotemporal GCIPL thickness = 66 μm), in an arcuate shape that does not cross the horizontal raphe. The superior RNFL defect does not invade the superior macular region, with the result that the superior macula is not damaged

Therefore, the RGC axons in the superior macula enter through the temporal border of the optic disc, while RGC axons in the inferior macula enter through the inferotemporal border of the optic disc. This topographical relationship between macula and optic disc results in an overlap of the inferior macular region with the inferotemporal region of the optic disc, where glaucomatous defects dominate. Hood et al. designated this region as the "macular vulnerability zone (MVZ)" of the optic disc (Fig. 2) (Hood et al. 2013; Hood 2017). Most of the RGCs in the inferior macular region project to the MVZ, which is the commonly affected region in glaucoma.

Kim et al. (2014a) further investigated the topographical relationship between localized peripapillary RNFL defect and macular GCIPL defect. They utilized the MATLAB program to construct a "GCIPL deviation frequency map" from 140 eyes of 140 open-angle glaucoma patients showing localized RNFL defect in one hemifield. According to the analysis from six different clock-hour locations of RNFL defect, the GCIPL defects had an arcuate shape that appeared as a continuation of the RNFL defect in the same hemisphere. The temporal macular region was the most frequently damaged site in either hemifield, and was larger in the inferior hemifield than in the superior (Fig. 3).

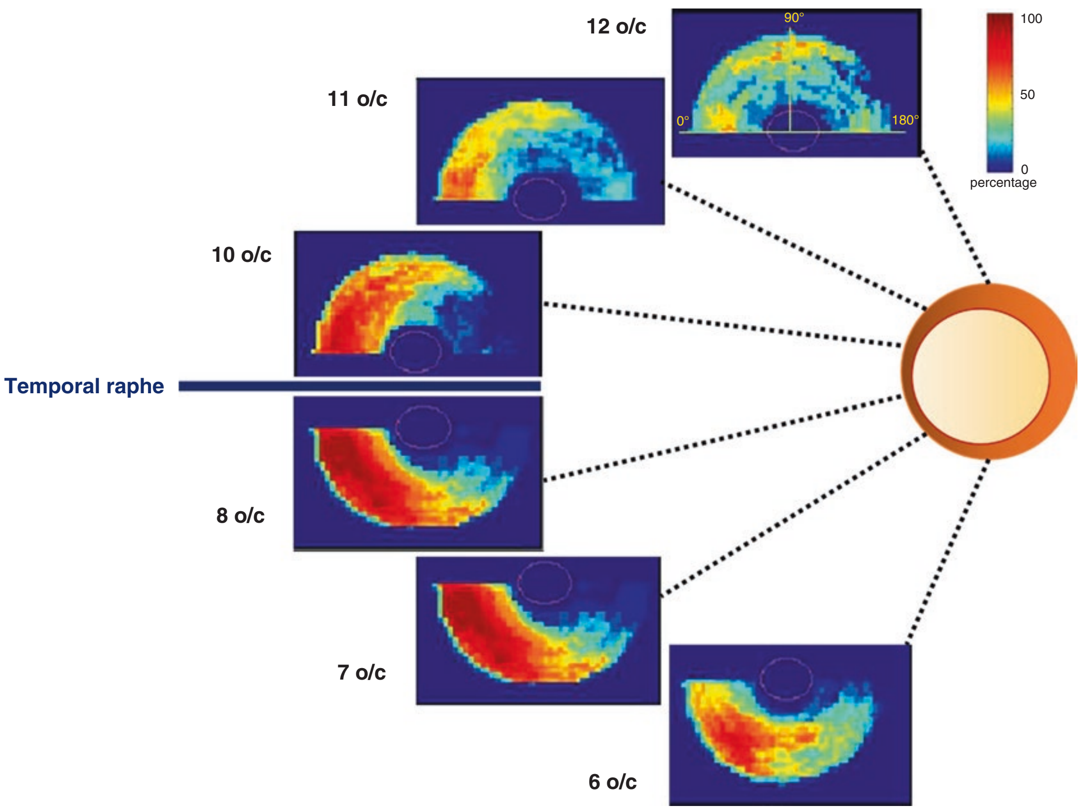

Fig. 3 Topographic relationship between localized peripapillary RNFL and macular GCIPL defects. A "GCIPL deviation frequency map" was constructed by superimposing the ganglion cell-inner plexiform layer (GCIPL) defects onto the deviation map corresponding to peripapillary retinal nerve fiber layer (RNFL) defects at different clock-hour locations (from 6 to 12 o'clock). The color-coded scale presents the frequency of GCIPL defects: the red-colored region indicates the highest GCIPL defect frequency, while the blue-colored region is close to zero. The GCIPL defects had an arcuate shape that appeared as a continuation of the RNFL defect in the same hemisphere. The temporal macular region was the most frequently damaged site in either hemifield, and was larger in the inferior hemifield than in the superior (adapted and modified from Kim et al. 2014a)

3 Diagnostic Accuracy of Macular Imaging

The macular parameters are known to have a high diagnostic utility for perimetric glaucoma comparable to those of peripapillary RNFL thickness or optic nerve head (ONH) parameters. In one study, the minimum (defined as the GCIPL thickness on the meridian showing the lowest average measurement) and inferotemporal GCIPL showed the highest sensitivity (94.8%) among GCIPL parameters, with comparable specificities (87.9 and 85.8%, respectively) (Mwanza et al. 2012). In another study, the GCC also showed good diagnostic utility for glaucoma comparable to that of peripapillary RNFL thickness, where global loss volume (percentage of global GCC loss over the entire GCC map) was found to be the best parameter (Tan et al. 2009).

3.1 Diagnostic Accuracy for Preperimetric and Early Glaucoma

Consistent with earlier studies investigating early-glaucomatous damage affecting the macula, the macular parameters have exhibited excellent RNFL-comparable diagnostic power for discriminating early-stage glaucoma (glaucoma suspect or preperimetric glaucoma). Mwanza et al. (2012) for the first time reported that minimum GCIPL thickness was found to be the best GCIPL parameter for discriminating early glaucoma (including both preperimetric and perimetric) from normal eyes. In a Korean study that had enrolled 92 preperimetric glaucoma patients and 92 age-matched controls, the inferotemporal GCIPL had comparable diagnostic power for glaucoma (area under receiver operating characteristic curves [AUROC] = 0.823), which results were not significantly different from those of the best parameter for peripapillary RNFL (7 o'clock sector, AUROC = 0.764) and ONH (rim area, 0.767) (Kim et al. 2014b). As the angular distance between the fovea and an RNFL defect increases, the sensitivity of macular GCIPL parameters for detection of RNFL defects deteriorates (Kim et al. 2014b; Hwang et al. 2014).

3.2 Diagnostic Accuracy in Myopic Eyes

Myopic eyes have divergent optic disc shapes such as are manifested in tilted disc, peripapillary atrophy, or posterior staphyloma. These structural variations make diagnosis and monitoring of glaucoma challenging in myopic eyes (Tan et al. 2019). Macular inner retinal thickness is known to be less affected by the degree of myopia and myopia-related ONH structural change relative to peripapillary RNFL thickness (Kim et al. 2015a; Jeong et al. 2016). In this context, macular GCIPL thickness can be an effective alternative method to evaluate glaucomatous damage in myopic eyes. A Korean study that included open-angle glaucoma patients with either highly myopic or non-highly myopic eyes reported that the best parameters for discriminating normal eyes from glaucomatous ones were inferior RNFL (0.906) and inferotemporal GCIPL (0.852) thickness in the highly myopic group, and average RNFL (0.920) and minimum GCIPL (0.908) thickness in the non-highly myopic group (Choi et al. 2013). Another Korean study further investigated inferotemporal GCIPL thickness's diagnostic utility in a myopic preperimetric glaucoma population, and found it to be the best parameter, having a significantly greater diagnostic power than the other parameters including average RNFL or GCIPL thickness, rim area, inferior RNFL thickness, and minimum GCIPL thickness (Seol et al. 2015). A recent study using swept-source OCT (SS-OCT, deep range imaging [DRI] OCT, Topcon, Tokyo, Japan) demonstrated that inferotemporal GCL+ (identical with GCIPL thickness) and GCL++ (identical with GCC thickness) had the greatest AUROC for myopic glaucoma (Kim et al. 2020). In this study, macular GCL++ thickness (87.6%) and GCL+ thickness (87.5%) showed greater AUROC than did macular GCIPL thickness based on spectral-domain OCT (Cirrus HD-OCT, Carl Zeiss Meditec, Dublin, CA, USA).

However, it should be noted that the macular parameters are not always dispositive in myopic eyes. The current normative database in most commercially available OCT devices does not fully represent the myopic population, with the result that the prevalence of false-positive red signs can reach 40.4% (Kim et al. 2015b). Myopic macular degeneration can cause abnormal thinning (due to patch atrophy) or thickening (due to retinoschisis) of the retinal layers, and these structural abnormalities may deteriorate the accuracy of OCT devices' automated segmentation (Tan et al. 2019; Ruiz-Medrano et al. 2019). Therefore, before interpreting macular parameters in glaucoma diagnostics, it would be prudent to carefully examine the entire macular structure and OCT scan quality rather than rely solely on the color-coded map and thickness profile.

4 Instrument-Specific Maps and Interpretation

4.1 Cirrus HD-OCT

Cirrus HD-OCT is an SD-OCT with a speed of 68,000 scans/s (latest model: Cirrus HD 6000) (Cirrus HD-OCT User Manual). It provides GCIPL thickness in a Ganglion Cell Analysis (GCA) printout. The GCIPL thickness is measured within a horizontally oval 4.8 × 4.0 mm area excluding a central perifoveal ellipse of 1.2 × 1.0 mm area: global average, minimum, and 6 wedge-shaped sectoral GCIPL thicknesses are provided in the GCA printout (Fig. 4). The normative database for macular measurements consists of 282 normal subjects aged between 19 and 84 years (mean: 46.5 years). Only 28 subjects aged 70–79 years and 3 subjects above age 80 are included therein, so caution is needed when interpreting patient data in these age ranges (Cirrus HD-OCT User Manual). There is no normative database for subjects younger than 19 years. Cirrus HD-OCT additionally provides an "Asian normative database" consisting of 315 individuals from Japan, China, and India (aged 19–79). All of these normative databases are adjusted only by age, and the color-coded maps in the GCA printouts do not take into account differences that may be present due to ethnicity, axial length, refraction, optic disc area, or signal strength (Cirrus HD-OCT User Manual).

Besides thickness measurements, the GCA printout provides additional GCIPL thickness and deviation maps. The thickness map provides the raw measurement thickness profiles on a color-scaled map. The deviation map shows regions wherein GCIPL thickness has fallen below the 5% limit based on the normative database with the yellow- (percentile values <5%) and red-color superpixels (percentile values <1%).

4.1.1 Temporal Raphe Sign

Temporal raphe sign (or GCIPL hemifield test) is determined to be positive in subjects who have a straight line on the horizontal raphe longer than one-half of the length between the inner and outer annulus in the temporal elliptical area of the GCIPL color thickness map (Fig. 5). This sign is known to be more effective than other macular parameters in discriminating early-glaucomatous changes (AUROC 0.967 in preperimetric glaucoma and 0.962 in perimetric glaucoma) (Kim et al. 2015c). This method is easy to apply in clinical practice and is advantageous for discrimination of glaucomatous change in highly myopic eyes that have a depigmented fundus and where RNFL defects are difficult to find (Kim et al. 2016). Temporal raphe sign positivity at the baseline has been associated with faster conversion to glaucoma in elderly subjects with a large cup-to-disc ratio (Ha et al. 2020).

4.1.2 PanoMap

Cirrus HD-OCT integrates the optic disc cube and macular cube scans into a single image and provides a combined wide-field OCT map, the so-called PanoMap (Fig. 6). The integration of the RNFL and GCIPL maps is useful for understanding the topographic patterns of glaucomatous structural damage in the early stages of glaucoma. By this method, Kim et al. (2017a) demonstrated that no single case of peripapillary RNFL defect in the MVZ was found without inferior macular GCIPL loss. However, there

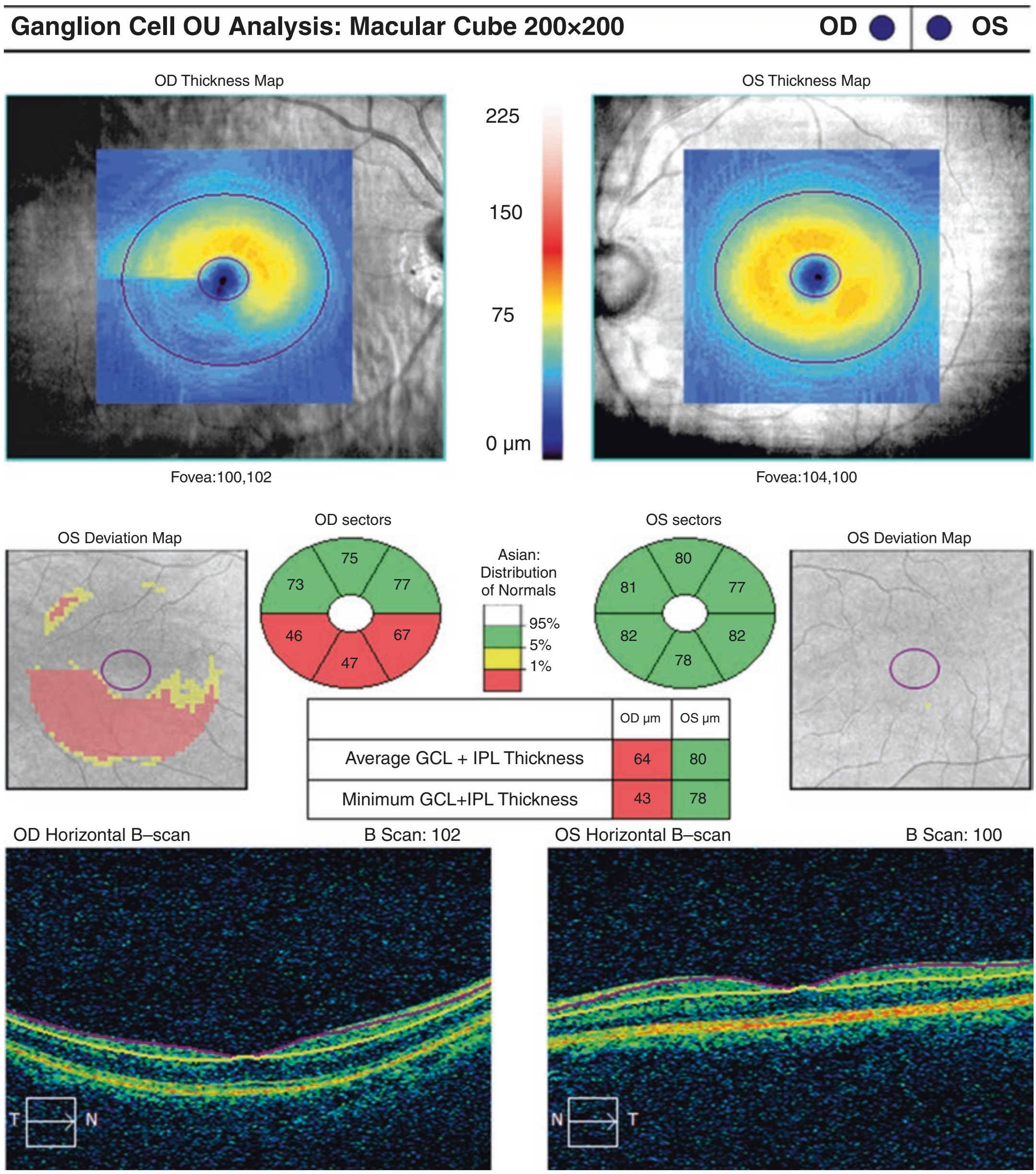

Fig. 4 Cirrus HD-OCT: Ganglion Cell Analysis. Typical printout of Ganglion Cell Analysis (GCA) from Cirrus HD-OCT. The thickness map (horizontally oval 4.8 × 4.0 mm area excluding central perifoveal ellipse 1.2 × 1.0 mm sized area) is provided in the first row. In the second row are the deviation maps showing regions where GCIPL thickness fell below the 5% limit based on the normative database with the yellow- (percentile values <5%) and red-color superpixels (percentile values <1%). Thickness measurements (average, minimum, and six sectoral measurements) with color-coded maps based on the internal normative database are provided in the center

were a few cases of inferior macular GCIPL loss without peripapillary RNFL defect in the MVZ. This finding suggests that inferior macular GCIPL loss may precede peripapillary RNFL defect in the MVZ. In Kim et al.'s (2017b) subsequent longitudinal observation of deviation maps of macular GCIPL and peripapillary RNFL from 151 eyes with early-stage glaucoma, macular

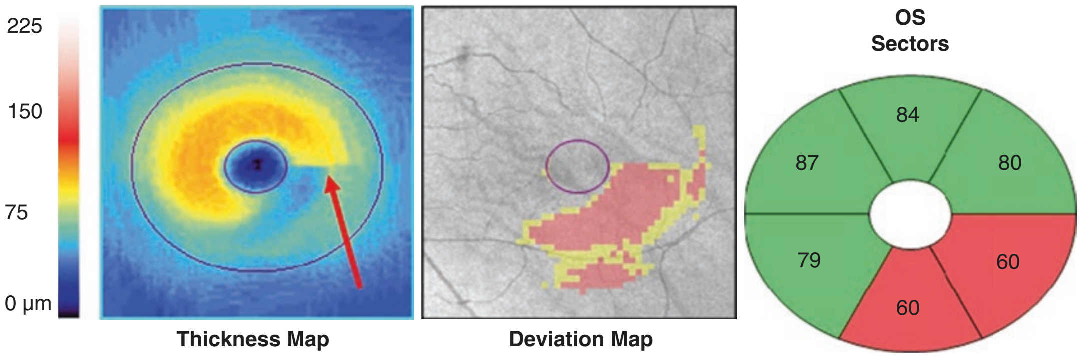

Fig. 5 Temporal Raphe sign. Temporal raphe sign (or GCIPL hemifield test) is determined to be positive in subjects who have a straight line longer than one-half of the length between the inner and outer annulus in the temporal elliptical area of the GCIPL color thickness map (red arrow). In this case, the patient has an inferotemporal retinal nerve fiber layer (RNFL) defect and a corresponding inferotemporal ganglion-cell inner plexiform layer (GCIPL) defect

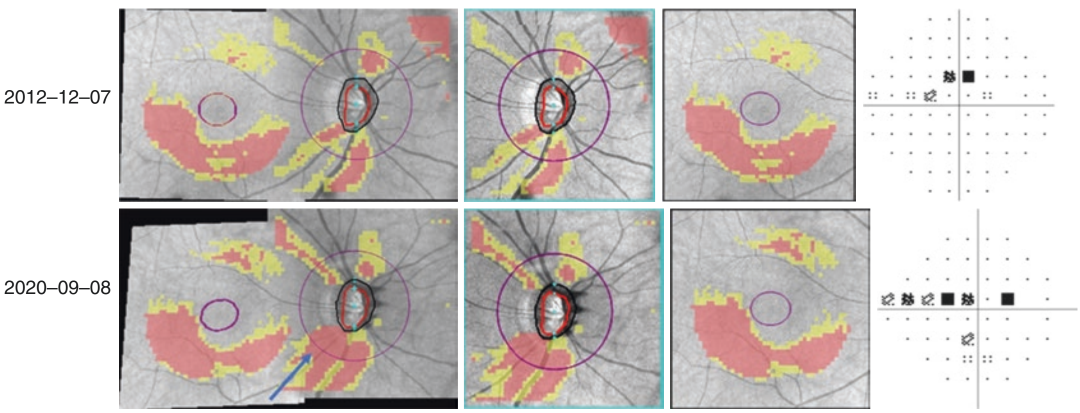

Fig. 6 PanoMap: combined GCA and RNFL deviation map. Cirrus HD-OCT PanoMap Analysis integrates data from optic disc cube and macular cube scans into a single image and provides a wide-field perspective for comprehensive posterior segment analysis. A case of 27-year-old male with myopia (spherical equivalence –5 diopters, axial length = 25.65 mm) and open-angle glaucoma in his right eye. At baseline (2012-12-07), the patient had inferoinferior retinal nerve fiber layer (RNFL) and inferotemporal ganglion-cell inner plexiform layer (GCIPL) defects. The automated perimetry showed a few superior paracentral scotomas (mean deviation, –2.14 dB). Eight years later (2020-09-08), the patient showed progressive thinning of the RNFL in the macular vulnerability zone (MVZ) (blue arrow) with increased nasal and paracentral scotomas

GCIPL change was frequently detected before corresponding peripapillary RNFL change (Fig. 6). Another study, this one from Australia, further demonstrated an association between lower intraocular pressure and glaucomatous structural change manifesting at the macular GCIPL before manifesting at the peripapillary RNFL (Marshall et al. 2019). These findings highlight the importance of macular imaging in glaucoma patients, as peripapillary RNFL analysis alone can overlook macular damage. The PanoMap is also known to be helpful in the detection of early-stage structural progression by inspecting various progression patterns of RNFL and GCIPL from a single combined image (Lee et al. 2018a, b).

4.2 Spectralis OCT

Spectralis OCT (Heidelberg Engineering GmbH, Heidelberg, Germany) has Glaucoma Module Premium Edition (GMPE) software that provides a Posterior Pole Asymmetry Analysis consisting of 61 horizontal B-scans, each comprised of 768 A-scans that are acquired along the Bruch's membrane opening (BMO)-fovea axis (Heidelberg Engineering). It provides a thickness map, a thickness deviation map, and a color-coded classification chart for the total retina, RNFL, GCL, and IPL (Fig. 7).

On the thickness deviation map, the red and yellow areas represent percentile values <1% and <5%, respectively, while the blue and purple areas represent percentile values >95% and >99%, respectively. The green areas represent a percentile value of 5–95%. There is no RNFL color-coded classification chart, because the macular RNFL is anatomically thin, which limits the reliability of measurements in this location, and also because RNFL defects are typically most prominent beyond the confines of the GCL-optimized grid (Heidelberg Engineering).

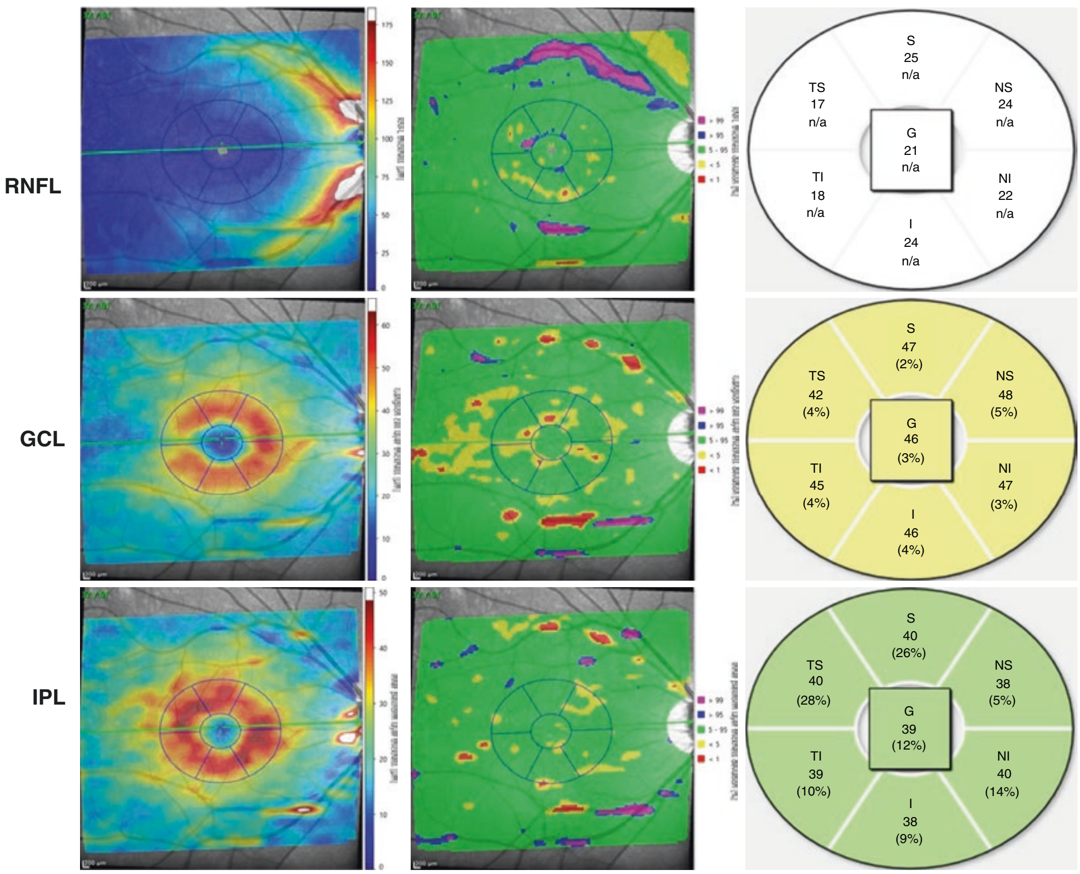

Fig. 7 Spectralis OCT: thickness and deviation maps. Spectralis OCT provides a thickness map, thickness deviation map, and color-coded classification chart for the total retina, retinal nerve fiber layer (RNFL), ganglion cell layer (GCL), and inner plexiform layer (IPL). In the thickness deviation map, the red and yellow areas represent percentile values <1% and <5%, respectively, while the blue and purple areas represent percentile values >95% and >99%, respectively. The green areas represent a percentile value of 5–95%. There is no RNFL color-coded classification chart, because the macular RNFL is anatomically thin, which limits the reliability of measurements in this location, and also because RNFL defects are typically most prominent beyond the confines of the GCL-optimized grid

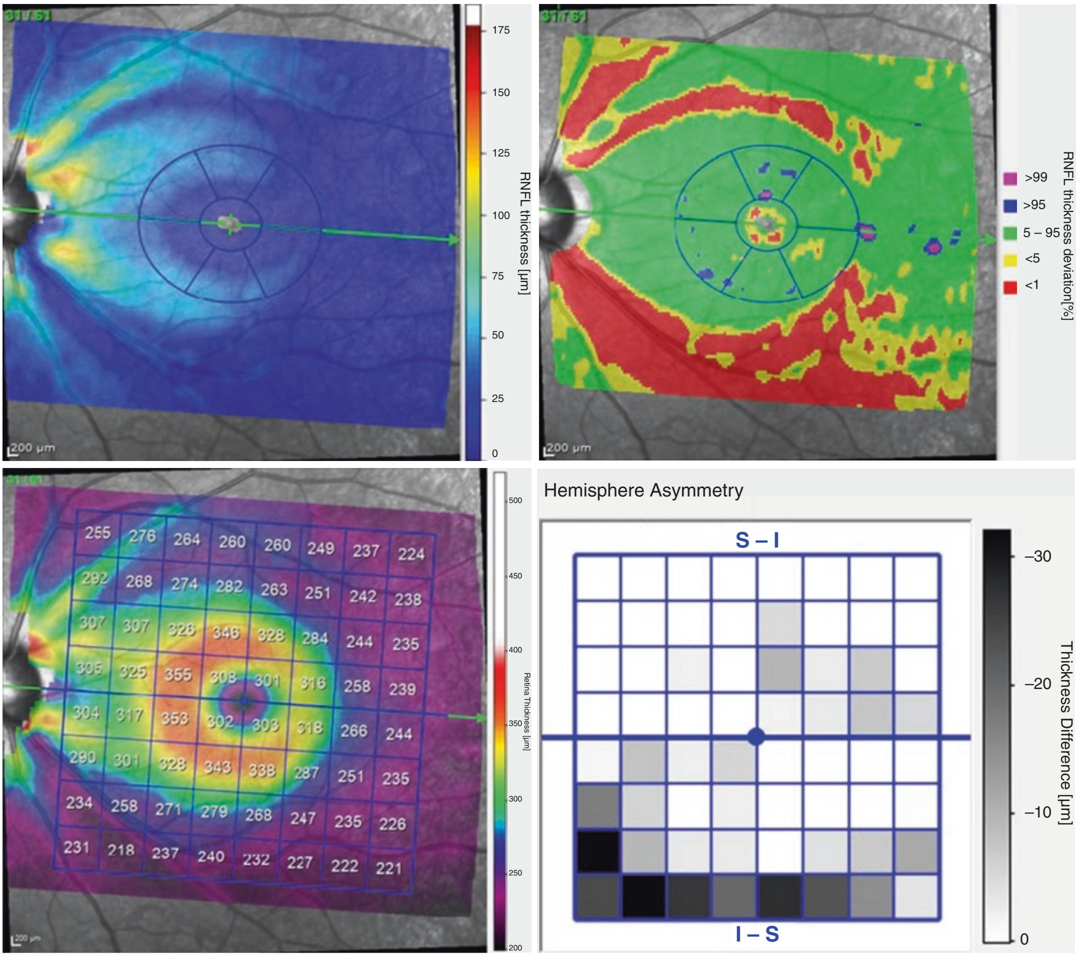

Fig. 8 Posterior pole asymmetry analysis. Spectralis OCT provides a retinal thickness asymmetry graph between the inferior and superior macula hemisphere of each eye. A case of 28-year-old male with open-angle glaucoma on his left eye. The patient had mild superotemporal and more severe inferotemporal retinal nerve fiber layer (RNFL) defects. The thickness asymmetry graph (bottom right) revealed asymmetrical retinal thinning in the inferior region

Total retinal thickness is further displayed on a color-coded map (Fig. 8). A thickness asymmetry graph between the inferior and superior macular hemispheres of each eye, and between the right and left eyes, is also available. The darker the square, the larger the difference in thickness between that square and the corresponding square in the opposite hemisphere or eye, with jet-black squares indicating a difference >30 μm.

4.3 DRI OCT Triton

DRI OCT Triton (Topcon, Tokyo, Japan) is a swept-source OCT using a longer, 1,050 nm wavelength light-source that enables a deeper imaging range and better tissue penetration. It provides a faster scanning speed of 100,000 A-scans/s, which significantly reduces motion artifacts with short capture times and collects

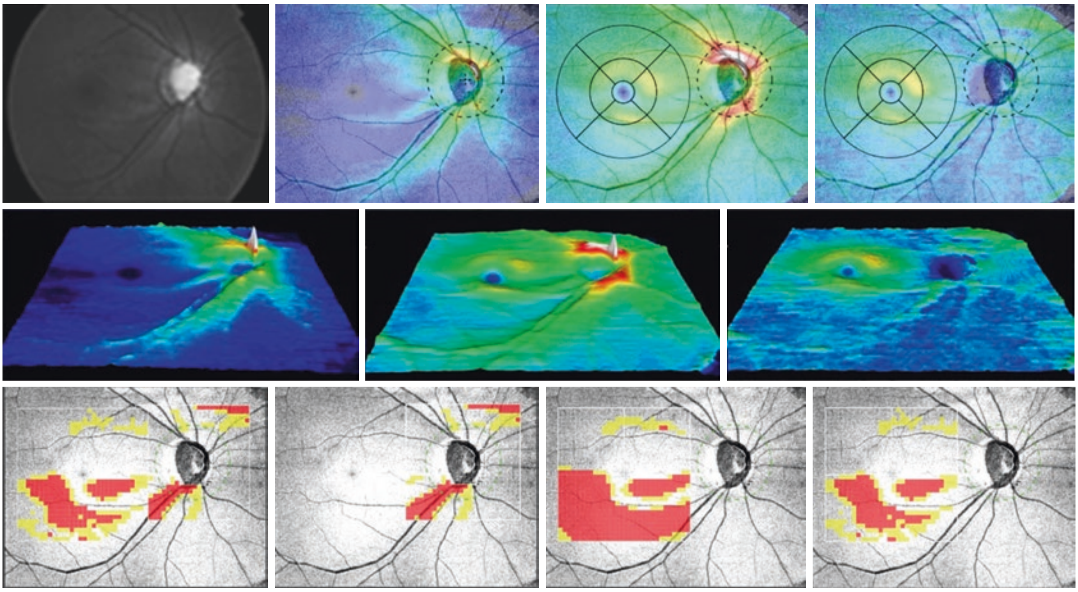

Fig. 9 DRI OCT Triton: wide-field map. The 3D Wide scan in DRI OCT Triton provides a 12 × 9 mm wide-field thickness map (first row), a thickness surface map (second row), and SuperPixel maps (third row) for the retinal nerve fiber layer (RNFL) (second column), GCL++ (third column), and GCL+ layers (fourth column). SuperPixel maps can be displayed as a combination of RNFL with either GCL++ or GCL+ (first column). The thickness surface map (second row) is displayed in 3D for selected layers (RNFL, GCL++, or GCL+, respectively), and can be rotated or zoomed-in and -out by mouse operation. The SuperPixel-200 map consists of 26 × 26 grids within a 5.2 × 5.2 mm^2 peripapillary area and 30 × 30 grids within a 6.0 × 6.0 mm^2 macular area, thereby providing a significance map based on the built-in normative database. The side length of each grid is 200 μm. The uncolored pixels indicate the normal range, whereas the yellow- and red-colored pixels indicate abnormality at P = 1–5% and P < 1% of the normal level, respectively

more OCT data in a single scan. The 3D Wide scan in DRI OCT Triton provides a 12 × 9 mm wide-field thickness map, a thickness surface map, and SuperPixel maps for the RNFL, GCL++, and GCL+ layers. The thickness surface map (second row) is displayed in 3D for selected layers (RNFL, GCL++, or GCL+) and can be rotated or zoomed-in and -out by mouse operation (Fig. 9). The SuperPixel-200 map consists of 26 × 26 grids within a 5.2 × 5.2 mm^2 peripapillary area and 30 × 30 grids within a 6.0 × 6.0 mm^2 macular area, thereby providing a significance map (identical with the deviation map in Cirrus OCT) based on the built-in normative database. The side length of each grid is 200 μm. Uncolored pixels indicate the normal range, whereas yellow- and red-colored pixels indicate abnormality at P = 1–5% and P < 1% of the normal level, respectively.

The inferior GCL++ (AUROC = 0.809) and inferotemporal GCL+ thickness (AUROC = 0.809) showed the greatest diagnostic ability for detection of preperimetric glaucoma from healthy eyes (Lee et al. 2017a). In addition, inferotemporal GCL++ (AUROC = 0.865) and GCL+ thicknesses (AUROC = 0.865) showed the best diagnostic power for early-perimetric glaucoma (Lee et al. 2017a). The wide-field thickness map showed comparable diagnostic power for preperimetric and early-perimetric glaucoma with Cirrus HD-OCT (Lee et al. 2018c). A recent study that enrolled 150 myopic primary open-angle glaucoma (POAG) eyes and 100 healthy myopic eyes reported that the RNFL/GCL++/GCL+ wide-field thickness (thickness surface) map showed better accuracy for glaucomatous defects in both the superotemporal and inferotemporal regions than did the Cirrus HD-OCT thickness map (Kim et al. 2020). This possibly was due to the difference in the measurement regions between the two devices. The measurement area of the macular parameter is within a 6 mm diameter circle for DRI OCT Triton and within a 4.8 × 4.0 mm elliptical annulus for Cirrus HD-OCT. A wider scan range in SS-OCT may be more advantageous for diagnosis of POAG in myopic eyes. Furthermore, the difference in the segmentation algorithms between the two OCT devices may influence the diagnostic power for myopic POAG (Kim et al. 2020; Pierro et al. 2012).

5 Detecting Glaucoma Progression

Monitoring of macular parameters facilitates detection of structural progression in glaucomatous eyes and prediction of subsequent visual field defect. The rate of GCIPL thinning reportedly is significantly faster in glaucomatous eyes with progression (Lee et al. 2017b, c). The mean rate of GCIPL thinning has been found to be significantly faster, even, in pseudoexfoliative glaucoma (–1.46 μm/year) than in open-angle glaucoma (–0.49 μm/year) or normal eyes (–0.31 μm/year) (Lee et al. 2019). A trend-based analysis (>5 years) of macular GCIPL and peripapillary RNFL from 163 POAG patients revealed that progressive macular GCIPL and peripapillary RNFL thinning were mutually predictive, and that both were indicative of visual field progression (Hou et al. 2018). Another retrospective cohort study, this one from Korea, also demonstrated that eyes with progressive GCIPL and RNFL thinning showed a significant higher risk of developing visual field defects (Shin et al. 2020).

Trend-based analysis of GCIPL is also known to be useful in detecting progression even in advanced-glaucoma eyes. Peripapillary RNFL is likely to reach the measurement floor in advanced-glaucoma eyes, which makes it less valuable for detection of progression in these eyes. However, recent studies reported significant rates of change for macular GCIPL but no significant changes for peripapillary RNFL or rim area in advanced-glaucoma eyes (Shin et al. 2017; Lavinsky et al. 2018). This suggests that damage impacting the macular GCIPL occurs at a different rate than in the case of the peripapillary RNFL.

References

Anctil JL, Anderson DR. Early foveal involvement and generalized depression of the visual field in glaucoma. Arch Ophthalmol. 1984;102(3):363–70.

Choi YJ, Jeoung JW, Park KH, Kim DM. Glaucoma detection ability of ganglion cell-inner plexiform layer thickness by spectral-domain optical coherence tomography in high myopia. Invest Ophthalmol Vis Sci. 2013;54(3):2296–304.

Cirrus HD-OCT User Manual 2660021159751 Rev. A 2015-08. Appendix A. https://www.zeiss.co.uk/content/dam/Meditec/gb/Chris/Refractive-Business-Builder/2018Updates/UserGuides/oct_usermanual.pdf. Accessed 25 Oct 2020.

Ha A, Kim YK, Kim JS, Jeoung JW, Park KH. Temporal raphe sign in elderly patients with large optic disc cupping: its evaluation as a predictive factor for glaucoma conversion. Am J Ophthalmol. 2020;219:205–14.

Heidelberg Engineering. Spectralis Glaucoma Toolkit. 10-4. https://business-lounge.heidelbergengineering.com/us/en/products/spectralis/glaucoma-module/downloads/#downloads. Accessed 25 Oct 2020.

Heijl A, Lundqvist L. The frequency distribution of earliest glaucomatous visual field defects documented by automatic perimetry. Acta Ophthalmol. 1984;62(4):658–64.

Hood DC. Improving our understanding, and detection, of glaucomatous damage: An approach based upon optical coherence tomography (OCT). Prog Retin Eye Res. 2017;57:46–75.

Hood DC, Raza AS, de Moraes CG, Liebmann JM, Ritch R. Glaucomatous damage of the macula. Prog Retin Eye Res. 2013;32:1–21.

Hou HW, Lin C, Leung CK. Integrating macular ganglion cell inner plexiform layer and parapapillary retinal nerve fiber layer measurements to detect glaucoma progression. Ophthalmology. 2018;125(6):822–31.

Hwang YH, Jeong YC, Kim HK, Sohn YH. Macular ganglion cell analysis for early detection of glaucoma. Ophthalmology. 2014;121(8):1508–15.

Jeong JH, Choi YJ, Park KH, Kim DM, Jeoung JW. Macular ganglion cell imaging study: covariate effects on the spectral domain optical coherence tomography for glaucoma diagnosis. PLoS One. 2016;11(8):e0160448.

Kim KE, Park KH, Yoo BW, Jeoung JW, Kim DM, Kim HC. Topographic localization of macular retinal ganglion cell loss associated with localized peripapillary retinal nerve fiber layer defect. Invest Ophthalmol Vis Sci. 2014a;55(6):3501–8.

Kim MJ, Jeoung JW, Park KH, Choi YJ, Kim DM. Topographic profiles of retinal nerve fiber layer defects affect the diagnostic performance of macular scans in preperimetric glaucoma. Invest Ophthalmol Vis Sci. 2014b;55(4):2079–87.

Kim MJ, Park KH, Yoo BW, Jeoung JW, Kim HC, Kim DM. Comparison of macular GCIPL and peripapillary RNFL deviation maps for detection of glaucomatous eye with localized RNFL defect. Acta Ophthalmol. 2015a;93(1):e22–8.

Kim KE, Jeoung JW, Park KH, Kim DM, Kim SH. Diagnostic classification of macular ganglion cell and retinal nerve fiber layer analysis: differentiation of false-positives from glaucoma. Ophthalmology. 2015b;122(3):502–10.

Kim YK, Yoo BW, Kim HC, Park KH. Automated detection of hemifield difference across horizontal raphe on ganglion cell—inner plexiform layer thickness map. Ophthalmology. 2015c;122(11):2252–60.

Kim YK, Yoo BW, Jeoung JW, Kim HC, Kim HJ, Park KH. Glaucoma-diagnostic ability of ganglion cell-inner plexiform layer thickness difference across temporal raphe in highly myopic eyes. Invest Ophthalmol Vis Sci. 2016;57(14):5856–63.

Kim YK, Jeoung JW, Park KH. Inferior macular damage in glaucoma: its relationship to retinal nerve fiber layer defect in macular vulnerability zone. J Glaucoma. 2017a;26(2):126–32.

Kim YK, Ha A, Na KI, Kim HJ, Jeoung JW, Park KH. Temporal relation between macular ganglion cell-inner plexiform layer loss and peripapillary retinal nerve fiber layer loss in glaucoma. Ophthalmology. 2017b;124(7):1056–64.

Kim YW, Lee J, Kim JS, Park KH. Diagnostic accuracy of wide-field map from swept-source optical coherence tomography for primary open-angle glaucoma in myopic eyes. Am J Ophthalmol. 2020;218:182–91.

Lavinsky F, Wu M, Schuman JS, Lucy KA, Liu M, Song Y, et al. Can macula and optic nerve head parameters detect glaucoma progression in eyes with advanced circumpapillary retinal nerve fiber layer damage? Ophthalmology. 2018;125(12):1907–12.

Lee WJ, Na KI, Kim YK, Jeoung JW, Park KH. Diagnostic ability of wide-field retinal nerve fiber layer maps using swept-source optical coherence tomography for detection of preperimetric and early perimetric glaucoma. J Glaucoma. 2017a;26(6):577–85.

Lee WJ, Kim YK, Park KH, Jeoung JW. Evaluation of ganglion cell-inner plexiform layer thinning in eyes with optic disc hemorrhage: a trend-based progression analysis. Invest Ophthalmol Vis Sci. 2017b;58(14):6449–56.

Lee WJ, Kim YK, Park KH, Jeoung JW. Trend-based analysis of ganglion cell-inner plexiform layer thickness changes on optical coherence tomography in glaucoma progression. Ophthalmology. 2017c;124(9):1383–91.

Lee WJ, Kim TJ, Kim YK, Jeoung JW, Park KH. Serial combined wide-field optical coherence tomography maps for detection of early glaucomatous structural progression. JAMA Ophthalmol. 2018a;136(10):1121–7.

Lee WJ, Na KI, Ha A, Kim YK, Jeoung JW, Park KH. Combined use of retinal nerve fiber layer and ganglion cell-inner plexiform layer event-based progression analysis. Am J Ophthalmol. 2018b;196:65–71.

Lee WJ, Oh S, Kim YK, Jeoung JW, Park KH. Comparison of glaucoma-diagnostic ability between wide-field swept-source OCT retinal nerve fiber layer maps and spectral-domain OCT. Eye. 2018c;32(9):1483–92.

Lee WJ, Baek SU, Kim YK, Park KH, Jeoung JW. Rates of ganglion cell-inner plexiform layer thinning in normal, open-angle glaucoma and pseudoexfoliation glaucoma eyes: a trend-based analysis. Invest Ophthalmol Vis Sci. 2019;60(2):599–604.

Marshall HN, Andrew NH, Hassall M, Qassim A, Souzeau E, Ridge B, et al. Macular ganglion cell-inner plexiform layer loss precedes peripapillary retinal nerve fiber layer loss in glaucoma with lower intraocular pressure. Ophthalmology. 2019;126(8):1119–30.

Mwanza JC, Durbin MK, Budenz DL, Sayyad FE, Chang RT, Neelakantan A, et al. Glaucoma diagnostic accuracy of ganglion cell-inner plexiform layer thickness: comparison with nerve fiber layer and optic nerve head. Ophthalmology. 2012;119(6):1151–8.

Pierro L, Gagliardi M, Iuliano L, Ambrosi A, Bandello F. Retinal nerve fiber layer thickness reproducibility using seven different OCT instruments. Invest Ophthalmol Vis Sci. 2012;53(9):5912–1920.

Ruiz-Medrano J, Montero JA, Flores-Moreno I, Arias L, García-Layana A, Ruiz-Moreno JM. Myopic maculopathy: Current status and proposal for a new classification and grading system (ATN). Prog Retin Eye Res. 2019;69:80–115.

Seol BR, Jeoung JW, Park KH. Glaucoma detection ability of macular ganglion cell-inner plexiform layer thickness in myopic preperimetric glaucoma. Invest Ophthalmol Vis Sci. 2015;56(13):8306–13.

Shin JW, Sung KR, Lee GC, Durbin MK, Cheng D. Ganglion cell-inner plexiform layer change detected by optical coherence tomography indicates progression in advanced glaucoma. Ophthalmology. 2017;124(10):1466–74.

Shin JW, Sung KR, Song MK. Ganglion cell-inner plexiform layer and retinal nerve fiber layer changes in glaucoma suspects enable prediction of glaucoma development. Am J Ophthalmol. 2020;210:26–34.

Tan O, Chopra V, Lu AT, Schuman JS, Ishikawa H, Wollstein G, et al. Detection of macular ganglion cell loss in glaucoma by Fourier-domain optical coherence tomography. Ophthalmology. 2009;116(12):2305–14.e1–2.

Tan NYQ, Sng CCA, Jonas JB, Wong TY, Jansonius NM, Ang M. Glaucoma in myopia: diagnostic dilemmas. Br J Ophthalmol. 2019;103(10):1347–55.